A&A 587, A147 (2016)
DOI: 10.1051/0004-6361/201527167

Astronomy & Astrophysics

A time domain experiment with *Swift*: monitoring of seven nearby galaxies

I. Andreoni[1,2,3], P. D'Avanzo[1], S. Campana[1], M. Branchesi[4,5], M.G. Bernardini[1], M. Della Valle[6,7], F. Mannucci[8], A. Melandri[1], and G. Tagliaferri[1]

[1] INAF, Osservatorio Astronomico di Brera, via E. Bianchi 46, 23807 Merate, Italy
e-mail: iandreoni@swin.edu.au
[2] Centre for Astrophysics and Supercomputing, Swinburne University of Technology, PO Box 218, Hawthorn VIC 3122, Australia
[3] Dipartimento di Fisica, Università Degli Studi di Milano, via Celoria 16, 20133 Milano, Italy
[4] INFN, Sezione di Firenze, via G. Sansone 1, 50019 Sesto Fiorentino, Italy
[5] Università degli Studi di Urbino "Carlo Bo", via A. Saffi 2, 61029 Urbino, Italy
[6] INAF, Osservatorio Astronomico di Capodimonte, salita Moiariello 16, 80131 Napoli, Italy
[7] ICRANET, Piazza della Repubblica 10, 65122 Pescara, Italy
[8] INAF, Osservatorio Astrofisico di Arcetri, largo E. Fermi 5, 50125 Firenze, Italy

Received 11 August 2015 / Accepted 12 January 2016

ABSTRACT

Context. Focused on the study of transient sources, time domain astronomy today is one of the most active and growing areas of research in astronomy. Most of the present and planned surveys aimed at carrying out time domain studies work in the optical band and founded their searching strategies on fixed cadences. Although nothing similar currently exists in the X-ray and ultraviolet (UV) bands, the *Swift* satellite is certainly the most appropriate available instrument to carry out such surveys.
Aims. We aimed to detect a supernova (SN) shock breakout (SBO) in nearby galaxies. The SBO marks the first escape of radiation from the blast wave that breaks through the photosphere of the star and launches the SN ejecta. The detection of an SBO is a diagnostic for the radius of the progenitor star and the ratio of explosion energy to ejecta mass. It also allows us to determine the onset of the explosion with an accuracy of a few hours to a few seconds.
Methods. Using the XRT and UVOT instruments onboard the *Swift* satellite, we carried out a weekly cadenced, six-month monitoring of seven nearby galaxies: NGC 1084, NGC 2207/IC 2163, NGC 2770, NGC 4303/M 61, NGC 3147, NGC 3690, and NGC 6754. We searched for variable or transient sources in the collected data. These galaxies were selected because they are close (distance ≤50 Mpc), small enough to fit in the *Swift*/UVOT field of view, and are hosts of at least three SNe in the past 20 yr.
Results. We found no evidence for an SN SBO event. Five objects located within the light of the sample galaxies were found to be variable in the X-ray and/or in the UV. These include mainly background active galactic nucleus and unresolved ULX in NGC 3690. In addition to these objects, we found two variable Galactic sources: the known nova CP Draconis (which experienced an outburst during our monitoring) and an uncatalogued eclipsing binary.
Conclusions. Despite the lack of SBO detections, the results of our explorative study encourage the use of *Swift* in further time domain studies. Moreover, since our sample galaxies are within the Universe volume that will be reached by the forthcoming advanced gravitational wave (GW) detectors (a-LIGO and a-Virgo), this work provides an example on how to carry out *Swift* surveys from which the GW signal from SNe can be detected, and to detect counterparts to GW triggers.

Key words. surveys – supernovae: general – gravitational waves

1. Introduction

Time domain astronomy is one of the most active and growing areas of research in astronomy because it is able to touch basically every aspect of this science with a different perspective. In the next decade, we expect it to flourish, prompted by facilities such as the Large Synoptic Survey Telescope[1] in the optical and the Low-Frequency Array for radio astronomy[2] and the Square Kilometre Array[3] in the radio. These facilities will revolutionise our understanding of the Universe with nightly searches of large swathes of sky for variable objects and a network of robotic telescopes ready to follow-up anything of interest in greater detail.

Time domain astronomy focuses on transient sources. These might be extragalactic, usually involving catastrophic events (supernovae are the most common examples) or Galactic, usually involving cataclysmic events (novae). In recent years, a few single-optical band surveys started exploiting the variable sky, such as the Catalina Sky Survey (Drake et al. 2009), the Palomar Transient Factory (Rau et al. 2009), the PanSTARRS (Stubbs et al. 2010), the La Silla Quest (Rabinowitz et al. 2011), the SUDARE at the VST (Botticella et al. 2013), and the SkyMapper (Keller et al. 2007) in the 1−2 m telescope category. These synoptic surveys concentrated on supernovae (SNe), leading for instance to the discovery of SN 2011fe in the Pinwheel galaxy

[1] lsst.org
[2] lofar.org
[3] skatelescope.org

M101 within ∼1 day of the explosion (Waagen 2011; Piro & Nakar 2014).

Facilities such as *Gaia*[4] in the optical, the Space Infrared Telescope Facility (*Spitzer*[5]) in the infra-red (with projects like SPIRITS; Kasliwal et al. 2013), the *Swift*[6], the Galaxy Evolution Explorer (GALEX[7]), and *Fermi*[8] at higher energies have been pioneers of time domain astronomy from space. They open the path to missions such as eROSITA[9] (although this is more focused on a "static" all-sky survey) and SVOM[10], which will monitor the high-energy sky in the near future.

A few thousand SNe have been discovered so far. These enhanced our understanding of the last stages of massive stellar lives and deaths, and led us to discover that we live in an accelerating Universe that may be dominated by dark energy. In the past few years, the decades-ago predicted pulses marking the precise moment that a supernova shock wave breaks out of the progenitor star were discovered (Campana et al. 2006; Soderberg et al. 2008). Longer duration (days) shock breakouts (SBOs) have been observed with GALEX by type II SNe related to larger (red giant) progenitors (e.g. Gezari et al. 2008; Schawinski et al. 2008). This is an important tool, since the direct detection of SN progenitors is incredibly difficult and has only been possible for a small number of nearby core-collapse SNe with pre-explosion high-resolution imaging. The *Swift* UltraViolet/Optical Telescope (UVOT, Roming et al. 2005) is particularly sensitive to the cooling envelope emission, which is bright in the UV for up to several days after the SBO and can provide estimates of the radius of the progenitor star.

Another ingredient in transient astronomy is the prospect of observing gravitational waves (GWs) in the next few years. The second-generation ground-based GW detectors are expected to reach a sensitivity that will enable detections of transient GW signals from coalescences of neutron star (NS) and/or stellar-mass black hole binary systems and from core-collapse of massive stars. The advanced LIGO (Aasi et al. 2015) and Virgo (Acernese et al. 2015) detectors in full sensitivity will observe coalescences of NSs up to a distance (averaged for sky location and system-orientation) of 200 Mpc. The core-collapse events are expected to be detectable within a few Mpc (Ott 2009; Müller et al. 2013; Ott et al. 2013; Gossan et al. 2015) and up to tens of Mpc for more optimistic models (Fryer & New 2011).

The present work focuses on SNe, which dominate among transient optical events in nearby galaxies (Rau et al. 2009). We aim at detecting the UV/X-ray SBO by monitoring nearby galaxies using *Swift*, which has previously proven its ability to redefine time domain astronomy with its instruments (Gehrels & Cannizzo 2015). While the UV/X-ray bright SBOs are directly possible electromagnetic (EM) counterparts of the GW signals from core-collapse events, nearby galaxies are in general the host of all the GW transient sources detectable by the GW detectors. This time domain experiment by *Swift* represents an example for a possible monitoring program to detect potential sources of GWs and at the same time to shed light on UV/X-ray "transient contaminants" in galaxy fields. Characterising transient events not directly associated with a GW event will be useful when the EM counterparts of compact object coalescences will be searched for in the future.

This paper is organised as follows. In Sect. 2 we describe our selection criteria for the galaxies and the monitoring characteristics. In Sect. 3 we describe the analysis procedures and in Sect. 4 our results. We discuss how well a weekly survey can determine SN SBO onsets in Sect. 5 and the role of such a survey in the search for EM counterparts to GW signals in Sect. 6.

2. Target galaxies and monitoring details

Our project aim is to monitor nearby galaxies that are the site of an intense production of SNe. In the selection of the targets one possible problem is dust obscuration. Typically, galaxies with a high star formation rate are heavily obscured by dust, making the SN detection problematic in the optical. For example, the large number of identified SNe in Arp 220 (IC 1127/IC 4553) came from the radio band, none were detected in the optical (Lonsdale et al. 2006), and Mannucci et al. (2003) showed that the core-collapse SN rate observed at near-IR wavelengths in starburst galaxies is about an order of magnitude higher than in the optical. For this reason, the selection of the sample cannot be based on the star formation rate alone. Hence we adopted a different approach, based on the number of observed SNe in nearby galaxies. Using the Asiago database (Barbon et al. 1999), we selected galaxies in which several SNe were already discovered. Requiring at least three observed SNe in the last 20 yr, we selected 11 galaxies (observed rate $\gtrsim$0.15 SN yr^{-1}). From these we excluded galaxies in the M 81/M 82 group because their separation is larger than the UVOT field of view. Our final selection criteria were that a) they are close (distance $\lesssim$50 Mpc, thus within the a-LIGO and a-Virgo horizon), which allows our instruments to resolve their internal structure, and that b) their angular size is small enough to fit within the field of view of the *Swift* telescopes (the field of view of the XRT is 23′ in diameter, or 0.12 deg^2, while the field of view of the UVOT is 17′ × 17′, or 0.08 deg^2).

With our selection criteria the final sample consists of ten galaxies. *Swift* observed seven of them over the period 2013–2014 (NGC 5468, NGC 6946, and NGC 4038 were left out). The sample is clearly not complete, but it provides a fair representation of nearby star-forming galaxies. We selected as target galaxies NGC 1084, the system NGC 2207/IC 2163, NGC 2770, NGC 4303/M 61, NGC 3147, NGC 3690, and NGC 6754. We present their main features in Table 1 and the details of the observations, such as the dates and the exposure times, in Tables A.1 to A.6. The monitoring has been carried out on a weekly timescale for about six months. We show examples of UV and X-ray images of the target galaxies in Figs. A.1 and A.2.

3. Analysis methods

We searched for transients in our dataset, along with increases in luminosity of permanent sources. UV images and X-ray images require different analysis methods, mainly because the angular resolution of the UVOT (∼1 arcsec) is better than the resolution of the XRT (∼15 arcsec) and the density of UV-optical sources largely overcomes the density of the X-ray sources. We used the latest version of the calibration files (CALDB) available in March 2013.

3.1. XRT data analysis

We processed the data with `xrtpipeline` v. 0.13.1 to derive calibrated event files. We searched for sources by adopting a

[4] `sci.esa.int/gaia/`
[5] `spitzer.caltech.edu`
[6] `swift.gsfc.nasa.gov`
[7] `galex.caltech.edu`
[8] `fermi.gsfc.nasa.gov`
[9] `mpe.mpg.de/eROSITA`
[10] `svom.frs`

Table 1. Selected targets with their right ascension (RA), declination (Dec), distance, apparent magnitude (V), and angular size.

Galaxy	RA(J2000)	Dec(J2000)	Dist (Mpc)	Mag (V)	Size (arcmin)
NGC 1084	02:45:59.926	−07:34:43.10	19	10.73	2.62 × 1.62
NGC 2770	09:09:33.622	+33:07:24.29	30	12.80	2.63 × 0.69
NGC 2207/IC2163	06:16:22.093	−21:22:21.80	40	10.65	4.84 × 3.29
NGC 4303/M 61	12:21:54.950	+04:28:24.92	15	9.65	4.64 × 3.48
NGC 3147	10:16:53.632	+73:24:02.34	44	10.61	2.85 × 2.33
NGC 3690	11:28:31.326	+58:33:41.80	45	12.86	1.61 × 1.41
NGC 6754	19:11:25.752	−50:38:31.96	42	11.14	2.40 × 0.91

Notes. Values provided by the SIMBAD and NED data repository.

signal-to-noise ratio threshold of $S/N = 3$. We took advantage of the HEAdas[11] software to identify sources, using the XIMAGE-`detect` tool. First, we searched in every single observation for objects exceeding the threshold. Then, we summed up all the observations of a single galaxy and again identified all significant sources. To build products for sources located outside our target galaxies, we took advantage of the *Swift*/XRT online tools[12] (Evans et al. 2009), while for the X-ray sources located inside the target galaxies we carried out a more careful analysis using HEAdas *XSELECT* (using circular apertures, radius = 20 arcsec, centred on each identified source).

One X-ray variable source (the nucleus of NGC 3147; see Sect. 4.5) displayed a count rate high enough to carry out a meaningful X-ray spectral analysis that enabled us to obtain a flux-calibrated light curve (Fig. 6). Using the *Swift*/XRT online tools, we extracted the 0.3-10 keV spectrum for every single epoch by fitting the data with an absorbed power-law model. The absorption component was fixed to the value of the Galactic column density $N_{\rm H}$ provided by Willingale et al. (2013). The results of our analysis are reported in Table A.7.

In the following, we consider sources relevant for our purposes if a) they have been detected above the $S/N = 3$ threshold in just a single (or a few) epoch; or b) their light curve cannot be satisfactorily fitted with a constant function (with a null-hypothesis probability from a constant fit threshold of $p < 0.01$).

3.2. UVOT data analysis

We observed with the UVOT/*uvm2* filter (central wavelength = 2246 Å, *FWHM* = 498 Å; Poole et al. 2008), which is the "purest" UV filter available (i.e. the filter with the smallest contamination from optical photons). We developed a semi-automatic algorithm based on the image subtraction to search for variable sources in the UVOT data. We took advantage of the ISIS (v. 2.2) (Alard & Lupton 1998; Alard 2000) and ESO-ECLIPSE (Devillard 1997) packages to perform the image subtraction and to handle the images. We extracted one image each per event file, corresponding to single observations. We aligned the images of a target galaxy taken at different epochs and generated a master image that is the median of all these aligned images. By subtracting this reference frame from every single image, we then searched for positive residuals in the image by looking for variable or new sources. We used the Source Extractor (Bertin & Arnouts 2010) to identify those residuals whose flux is greater than five times the standard deviation of the local background of the subtracted image. We required the residuals to be symmetric (i.e. related to a point-like source) and with a full width at half maximul (FWHM) comparable to the FWHM of the UVOT (i.e. ∼5 arcsec), assuming a symmetrical PSF. For each potentially varying sources, we used the HEAdas `uvotproduct` tool to build its UV light curve using apertures with radius =3 arcsec. The conversion ratio of count rate to flux was obtained using the UVOT photometric system (Breeveld et al. 2011). No correction for MW reddening was applied in the derived light curves.

[11] `heasarc.nasa.gov/docs/software/lheasoft/`
[12] `swift.ac.uk/user_objects/`

4. Results

In summary, during our monitoring of seven nearby galaxies with the *Swift* XRT and UVOT telescopes we have detected

- one variable X-ray source inside the galaxy NGC 1084 (NGC 1084-I1, see Sect. 4.1), which was likely generated by one to three active galactic nuclei (AGNs) at higher redshift;
- one low-luminosity AGN at the centre of the galaxy NGC 4303 (NGC 4303-I1, see Sect. 4.4) and one at the centre of NGC 3147 (NGC 3147-I1, see Sect. 4.5), both variable in the X-rays but not in the UV band;
- one variable X-ray source inside the galaxy NGC 3690 (possibly due to the unresolved emission of a number of point-like sources detected by *Chandra* and positionally coincident with NGC 3690-I1, see Sect. 4.6);
- one Seyfert 1 galaxy located in a region of the sky outside NGC 4303 (NGC 4303-O1, see Sect. 4.4) variable in the X-rays as well as in the UV band;
- one possible quasar in a region of the sky outside the target galaxy NGC 3147 (NGC 3147-O2, see Sect. 4.5), variable in the X-rays but outside the field of view of the UVOT;
- a Galactic uncatalogued eclipsing binary, located in a region of the sky outside the target galaxy NGC 2770 (NGC 2770-O1, see Sect. 4.3);
- a Galactic known nova (CP Draconis) outside the target galaxy NGC 3147 (NGC 3147-O1, see Sect. 4.5).

We found two false positives in our UVOT dataset, that is to say, we identified two sources that survived our selection criteria but that we classified as spurious, ghost images. In one case the ghost lies very close to a bright star, in the other one it is right at the border of the image, where spurious events generated by instrumentation are more likely to happen.

We now discuss the results of the analysis of each target galaxy.

4.1. NGC 1084

The galaxy NGC 1084 was monitored weekly from the beginning of November 2013 to the second week of March 2014. Good data have been collected for 20 epochs by the XRT and

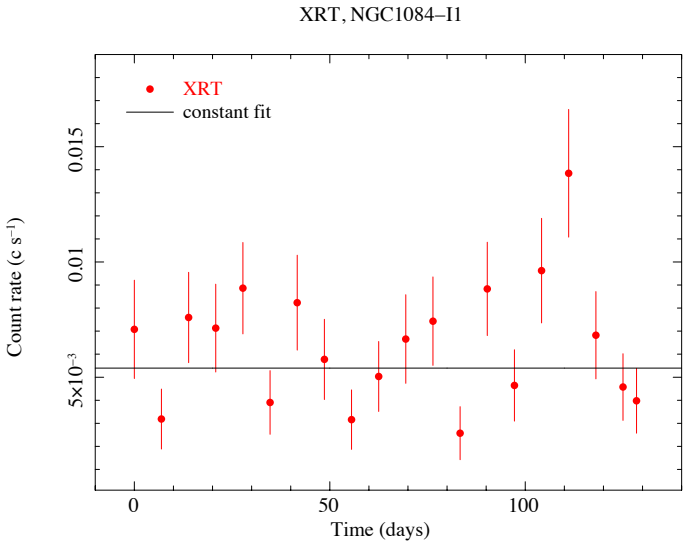

Fig. 1. X-ray emission detected from NGC 1084-I1. The time zero is set to mission elapsed time (MET) = 405027281 s (2013-11-01). We extracted this light curve using an aperture with radius 20 arcsec. The fit performed on the data with a constant function returns a mean count rate of 5.4×10^{-3} counts s^{-1}. A fit with a constant function gives a $\chi^2 = 40.2$ (for 19 degrees of freedom, d.o.f.), and $p = 0.0031$.

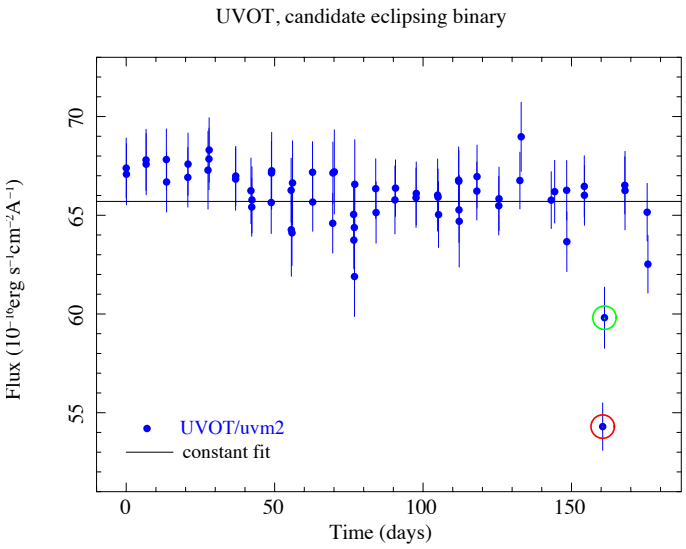

Fig. 2. UVOT/*uvm2* light curve of the candidate eclipsing binary system NGC 2770-O1. The time zero is set to MET = 408372298 s (2013-12-10). The fit performed on the data with a constant function returns a mean flux of 6.6×10^{-15} erg s^{-1} cm^{-2} A^{-1}. The fit provides a $\chi^2 = 147.1$ (63 d.o.f.) and a probability $p = 9 \times 10^{-11}$. The flux suddenly decreases by ∼20% (red circle) and ∼10% (green circle) with respect to the constant value. Both points were collected on May 20, 2014, in two different orbits of the *Swift* satellite. We found no X-ray counterpart to this source.

for 19 epochs by the UVOT (see Table A.1). We found no transient events in the UVOT data. In the XRT data we found that the light curve of an extended region (centred on RA = 02:45:59.9, Dec = –07:34:23.3, named NGC 1048-I1[13]) located inside the target galaxy NGC 1084 varies significantly (Fig. 1). We note, however, that three candidate AGN (Brough et al. 2006; Cavuoti et al. 2014) stand within the region, possibly causing the observed variability. We found no significant variability in the UVOT data inside the same region, nor in smaller regions around each AGN.

4.2. NGC 2207/IC 2163

The system NGC 2207/IC 2163 was monitored weekly from the beginning of November 2013 to the end of April 2014. Good data have been collected for 27 epochs by the XRT and for 26 epochs by the UVOT (see Table A.2). We found no transient events in the UVOT or the XRT data.

4.3. NGC 2770

The galaxy NGC 2770 was monitored weekly from the second week of December 2013 to the beginning of June 2014. Good data have been collected for 25 epochs by both the XRT and the UVOT (see Table A.3). In the UVOT data we found no transient events that could be interesting to our purposes. However, we identified a sudden drop of the UV flux emitted by a star outside the target galaxy. This source is located at coordinates RA = 9:09:34.8, Dec = +33:09:28.4 (NGC 2770-O1). Its light curve keeps a constant trend until the flux suddenly decreases in two consecutive points (both occurring on May 20, 2014, as they correspond to two different orbits of the *Swift* satellite) by ∼20% and ∼10 % with respect to the mean value (Fig. 2). This source is classified as an $r = 12$ mag star in the SDSS. We have not detected any X-ray counterpart to this source in our XRT dataset. We suggest that it may be an eclipsing binary system. In the XRT data we found no transient events and no variability inside or outside the galaxy NGC 2770.

4.4. NGC 4303/M 61

The galaxy NGC 4303 – better known as M 61 – was monitored weekly from the final week of January 2014 to the first week of June 2014. Good data have been collected for 21 epochs by the XRT and for 20 epochs by the UVOT (see Table A.4). This galaxy hosts a low-luminosity AGN (Brinkmann et al. 1994). We detected no transient events in the UVOT data. The X-ray emission of the active nucleus is significantly variable, as expected (Fig. 3). The flux of its UV counterpart does not vary significantly in the same time frame. As for the other galaxies, we analysed the X-ray sources located outside the target galaxy. One of them (NGC 4303-O1) shows significant variability in its light curve (Fig. 4). The source is coincident with a known Seyfert 1 galaxy (RA = 12:21:38.0, Dec = +04:30:26.4, Spinelli et al. 2006). We found in the UVOT data that its counterpart at lower energy is also highly variable (Fig. 4). This UV variability has not been detected by our algorithm during the UVOT data analysis because we optimised the procedure for point-like sources inside nearby galaxies. In this case, the variable emission comes from the unresolved nucleus of an extended source, which leads the image subtraction to produce an asymmetrical residual that was discarded by our automatic procedure.

In October 2014 the type Ia supernova SN 2014dt exploded in M 61 (Nakano et al. 2014; Ochner et al. 2014). We monitored this galaxy with the *Swift* satellite until the first week of June 2014 (Table A.4). Our dataset lacks any precursor signal that can be related to SN 2014dt, both in the X-rays and in the UV band. We also found no evidence of any luminous progenitor, in agreement with Foley et al. (2015).

[13] All coordinates here and in the following refer to J2000.

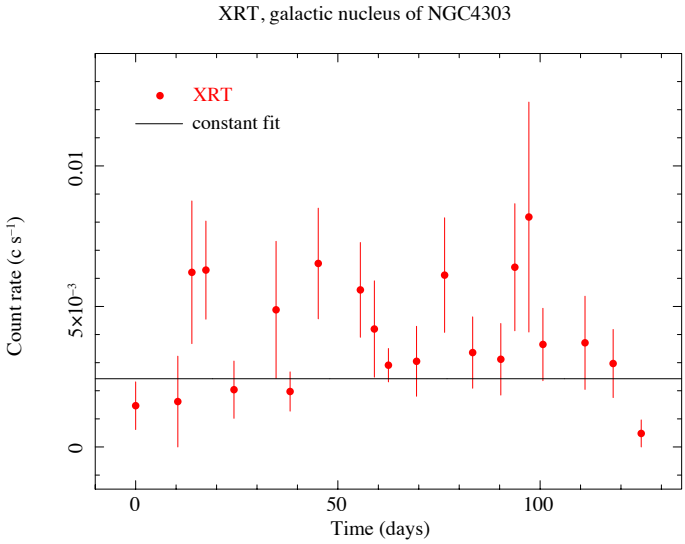

Fig. 3. X-ray light curve of the galactic nucleus of NGC 4303. The time zero is set to MET = 412217321 s (2014-01-24). The fit performed on the data with a constant function returns a mean rate of 2.4×10^{-3} counts s^{-1} (χ^2 = 47.30 for 20 d.o.f. and p = 0.0005). No significant UV variability is present in our dataset.

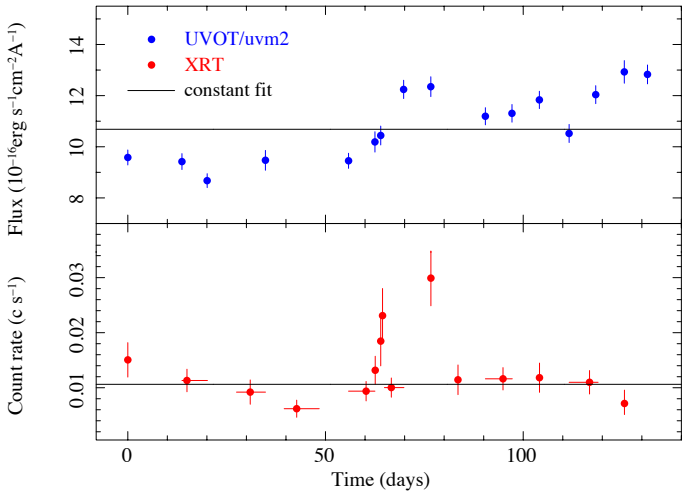

Fig. 4. UVOT/*uvm2* and XRT light curves of the NGC 4303-O1, identified as a Seyfert 1 galaxy (catalogued as 2XMM J122137.8+043025). The time zero is set to MET = 412217321 s (2014-01-24). The fit performed on the data with a constant function returns a mean UV flux (*upper panel*, aperture with radius = 5 arcsec) of 1.1×10^{-15} erg s^{-1} cm^{-2} A^{-1}, χ^2 = 242.8 (15 d.o.f.), and a null probability. The fit with a constant function on the X-ray data (*lower panel*) returns a mean rate of 1.06×10^{-2} counts s^{-1}, χ^2 = 39.15 (14 d.o.f.), and p = 0.0003.

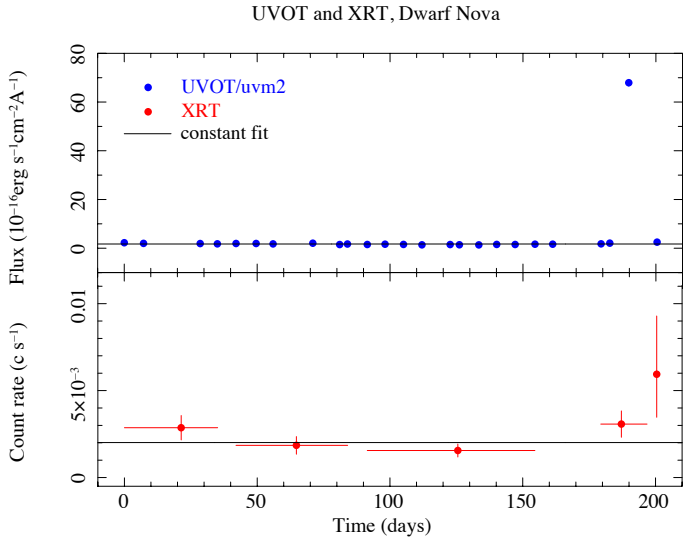

Fig. 5. UVOT/*uvm2* light curve (*upper panel*) extracted with an aperture (radius = 6 arcsec) centred on the dwarf nova CP Draconis (NGC 3147-O1). The time zero is set to MET = 409627840 s (2013-12-25). The fit with a constant function provides a χ^2 = 3685 (25 d.o.f.), and a null probability. The X-ray counterpart to this source (*lower panel*) does not show any significant variability, as the fit with a constant function returns a χ^2 = 6.426 (4 d.o.f.) and a probability p = 0.1695.

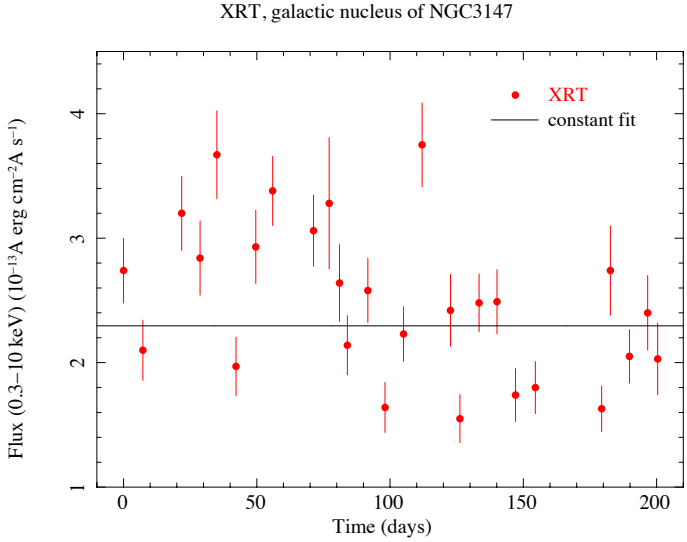

Fig. 6. X-ray light curve of the AGN (Ptak et al. 1996) of NGC 3147 (NGC 3147-I1). We detected enough photons from this source to build a spectrum at each epoch and convert the count rate to flux. The spectral indexes found at each epoch are listed in Table A.7. The time zero is set to MET = 409627840 s (2013-12-25). The mean flux is 2.3×10^{-13} erg cm^{-2} s^{-1}. The fit with a constant gives χ^2 = 141.6 (26 d.o.f.) and a null probability. The UV counterpart of this source is not significantly variable.

4.5. NGC 3147

The galaxy NGC 3147, a Seyfert 2 galaxy hosting an AGN (Ptak et al. 1996), was monitored weekly from the final week of 2013 to the second week of July 2014. Good data have been collected for 27 epochs by both the XRT and the UVOT (see Table A.7). We have detected one transient event (a known dwarf nova, located outside the target galaxy) in our UVOT dataset, at coordinates RA = 10:15:39.8, Dec = +73:26:05.0. We identified the outburst of the dwarf nova CP Draconis (NGC 3147-O1) in the observation of July 2, 2014. The outburst activity of this object is known to be recurrent (Shears et al. 2011). The UV light curve (Fig. 5, upper panel) shows that the flux rises to at least $(6.79 \pm 0.13) \times 10^{-15}$ erg s^{-1} cm^{-2} A^{-1} during the outburst, while it lies around $\sim 1.4 \times 10^{-16}$ erg s^{-1} cm^{-2} A^{-1} during the quiescent phase. The X-ray counterpart to this source (Fig. 5, lower panel) consists of a weak signal that shows no significant variability during our monitoring.

In the XRT data we found two variable sources. The first, as expected, is the active nucleus of NGC 3147 (Fig. 6),

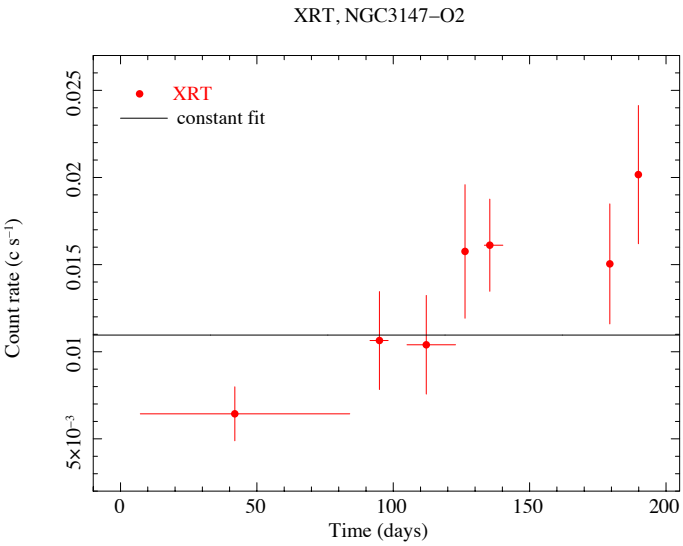

Fig. 7. XRT light curve of the candidate quasar (Flesch 2010) (NGC 3147-O2). The time zero is set to MET = 409627840 s (2013-12-25). The mean rate is 1.10×10^{-2} counts s^{-1}, $\chi^2 = 20.73$ (6 d.o.f.) and $p = 0.0021$.

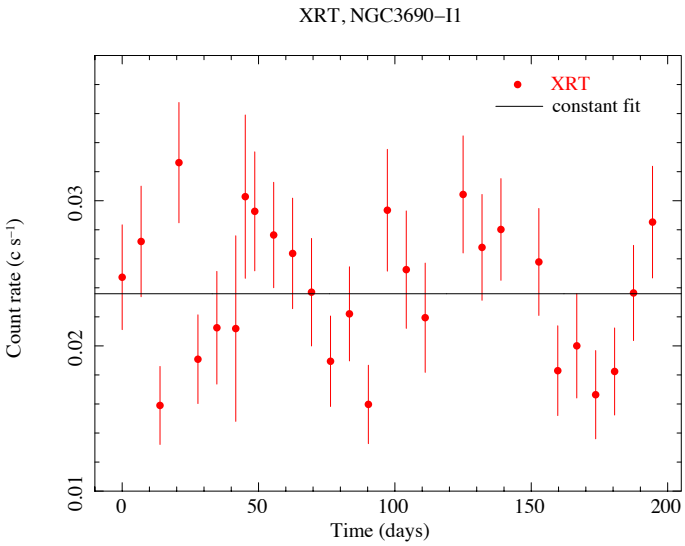

Fig. 8. X-ray radiation detected inside the target galaxy NGC 3690 (NGC 3690-I1). This galaxy is not characterised by an active nucleus, so the radiation is likely generated by a number of X-ray emitters inside the galaxy. The time zero is set to MET = 411013065 s (2014-01-10). The fit performed on the data with a constant function returns a rate of 2.36×10^{-2} counts s^{-1}, a $\chi^2 = 62.85$ (35 d.o.f.) and $p = 0.0026$.

NGC 3147-I1. Its variability in the UV band is negligible, however. The second variable X-ray source, NGC 3147-O2, is a candidate quasar (RA = 10:14:21.5, Dec = +73:17:26.0, Flesch 2010), located outside the target galaxy, but too far from NGC 3147 to fit within the UVOT field of view.

4.6. NGC 3690

The galaxy NGC 3690 was monitored weekly from the second week of January 2014 to the last week of September 2014. Good data have been collected for 35 by the XRT and for 34 epochs by the UVOT (see Table A.5). We identified no transient events in the UVOT data collected during our observations. In the XRT data we identified a powerful and significantly variable emission generated inside the target galaxy NGC 3690 at coordinates RA = 11:28:31.7, Dec = +58:33:46.4 (NGC 3690-I1, see Fig. 8). Several X-ray sources are present within NGC 3690, as observed by *Chandra* (Zezas et al. 2003) and *NuSTAR* (Ptak et al. 2015) at a position consistent with our variable X-ray source. Two of them have been identified as AGNs, some others might be classified as ultra-luminous X-ray sources (ULX). Considering the angular resolution of the XRT, we cannot conclude which source(s) is responsible for the observed variability.

4.7. NGC 6754

The galaxy NGC 6754 was monitored weekly from the first week of April 2014 to the end of September 2014. Good data have been collected for 27 epochs by both the XRT and the UVOT (see Table A.6). We found no transient events in the UVOT or in the XRT data.

5. Supernova shock breakouts

The SBO, that is, the soft X-ray and UV outburst expected at the birth of SNe (Colgate 1974; Falk 1978; Chevalier & Klein 1978; Matzner & McKee 1999), marks the first escape of radiation when the blast wave breaks through the surface of the star and launches the SN ejecta. Its detection can enable an early follow-up of the SN, with a detailed study of the luminosity and temperature evolution of the early thermal expansion phase. This information can be used as a diagnostic for the radius of the progenitor star and of the ratio of the explosion energy to the ejecta mass (Waxman et al. 2007).

The short duration (seconds to hours) of SBOs and the lack of sensitive wide-field searches at high energies make discovering them very hard. However, the *Swift*/XRT and UVOT provided evidence of their existence by detecting the early X-ray/UV emission a few days before SNe 2006aj associated with the GRB 060218 (Campana et al. 2006) and before SNe 2008D (Soderberg et al. 2008). The GALEX satellite detected serendipitous early UV events associated with SNe SNLS-04D2dc (Schawinski et al. 2008; Gezari et al. 2008), SNLS-06D1jd (Gezari et al. 2008), and 2010aq (Gezari et al. 2010).

These few observations demonstrate that it is possible to constrain the onset time (T_0) of SBOs, which marks the moment of the star explosion. For red supergiant progenitors (radius $\sim 10^{13}$ cm, then Type II-P SNe), T_0 was estimated with 0.75 day accuracy for SNLS-06D1jd and 0.35 days for SNLS-04D2dc (Gezari et al. 2008), while Schawinski et al. (2008) was able to estimate it with a precision of ~1 h. A 0.02 day accuracy was reached for SN 2010aq (Gezari et al. 2010) by fitting the data with theoretical models (Rabinak & Waxman 2011). For Wolf-Rayet star progenitors (radius $\sim 10^{11}$ cm, then Type Ibc SNe), the onset of the X-ray SBO associated with SN 2008D (Soderberg et al. 2008) was determined with an accuracy of 9^{+8}_{-20} s. A precise determination of the (T_0), achieved with SBO observations and accurate theoretical models describing how the shock wave propagates through the exploding star, is fundamental in the multi-messenger studies, which use SBOs as triggers to search for GWs and neutrinos (see Sect. 6).

The effectiveness of our survey to detect an SBO was estimated to be $15.9^{+11.1}_{-6.6}$% from Type II-P SNe and 0.03% (±0.02%) from Type Ibc SNe. To calculate these probabilities, we assumed a (conservative) detection rate of three SNe in the last 20 yr

(0.15 SNe yr^{-1}) for each galaxy of our sample (Barbon et al. 1999), with a 90% interval corresponding to a Poissonian mean rate of (0.08−0.27) SNe yr^{-1}. We considered the UV emission to last for 3.5 days and 1000 s for Type II-P and Tipe Ibc SNe, respectively. We also accounted for 65% of the SNe that explode as Type II-P and the 25% that explode as Type Ibc (Smartt 2009; van den Bergh et al. 2005; Cappellaro et al. 1999).

6. Counterparts to gravitational waves

The multi-frequency periodic monitoring of nearby galaxies presented in this paper represents a useful explorative study to test the capabilities of the *Swift* satellite for joint surveys with the GW detectors. Our target, the SBO, is an expected EM counterpart to GW signals from core-collapse SNe, and our sample galaxies are within the Universe volume (<200 Mpc) that will be reached by the forthcoming advanced GW detectors (a-LIGO and a-Virgo) for binary coalescing NS systems.

Two types of multi-messenger searches can benefit from this type of *Swift* survey: the search that uses external EM trigger events to search for gravitational wave events (e.g. Abadie et al. 2012a) and the EM follow-up of GW candidate events (e.g. Abadie et al. 2012b).

The *Swift* detection of a transient phenomenon that is expected to be a GW emitter, such as local (within few tens of Mpc) SNe or "orphan" gamma-ray bursts (Ghirlanda et al. 2015), provides timing and sky position that can be used in the search for the GW signal. The use of external triggers improves the GW search sensitivity significantly (Wąs et al. 2012) with respect to all-sky searches. The probability of detecting SNe during a *Swift* monitoring like the one of the present work does not significantly increase the total number of local SNe detected by optical surveys that can be used as external triggers. However, the X-ray/UV detection can give a more precise way to estimate the explosion time T_0 and the time window (T_0 uncertainties) within which to search for the GW signal. As discussed in the previous section, the detection of an SBO associated with accurate theoretical models permits estimating the time of the core-collapse (and thus of the GW emission) with precision from hours down to seconds. On the other hand, the detection of a "canonical" SN or gamma-ray burst afterglow, even with a frequent (daily) monitoring, will likely not provide an estimate of T_0 with a precision better than one day.

The narrow field of the *Swift*/XRT and UVOT limits the search for the EM counterpart to a GW source because even in the era of the advanced detectors, the sky localisation uncertainty of GW signals is expected to be large (hundreds of square degrees, Singer et al. 2014; Aasi et al. 2013). For this reason, the effective strategy for the *Swift* satellite is to observe a limited number of fields inside the error region, namely those containing known nearby galaxies (Evans et al. 2012, 2016; Kanner et al. 2012; Gehrels & Cannizzo 2015).

Any search for EM counterparts to GW signals needs to solve the problem of contamination from variable or transient objects that are unrelated with the GW source, but are detected within its localisation region (e.g. Cowperthwaite & Berger 2015). In our six-month monitoring (weekly cadenced) of seven close-by galaxies, we found that the main contaminant (variable) sources in both X-rays (limiting flux $\sim 1.3 \times 10^{-13}$ erg s^{-1} cm^{-2}) and UV (limiting flux $\sim 1.5 \times 10^{-13}$ erg s^{-1} cm^{-2}) are AGNs (NGC 1084-I1, NGC 4303-I1, NGC 3147-I1) and likely ULX (NGC 3690-I1), if the search is limited to within the galaxies. For these events, the use of astronomical catalogues (mainly through the Vizier database[14]) was sufficient to securely identify most of them, both in X-rays and in UV. This suggests that an automated and rapid use of archival data will be extremely useful to reduce the contaminants.

In our survey of seven galaxies covering a sky area 0.014 deg^2, no other contaminant brighter than 3×10^{-12} erg s^{-1} cm^{-2} (0.2−2 KeV band) was found. Kanner et al. (2013) estimated 4×10^{-4} transients per square degree with a flux brighter than the above threshold, spatially coincident with galaxies, and after rejecting previously identified AGNs. According to Poissonian statistics, the probability of observing zero transients in our small observed area is approximately 1.

7. Conclusions

We have observed seven nearby galaxies with a weekly cadence for about six months over the period 2013-2014 with the *Swift*/UVOT and XRT. Aiming at the detection of an SN SBO, we chose to target nearby galaxies with high rate of SNe recently detected in the optical (≥three SN in the last 20 yr): NGC 1084, the system NGC 2207/IC 2163, NGC 2770, NGC 4303/M 61, NGC 3147, NGC 3690, and NGC 6754. We estimated the probability of detecting an SBO (including the cooling phase) during our survey to be $15.9^{+11.1}_{-6.6}$% for Type II-P SNe, 0.03% (±0.02%) for Type Ibc SNe. We detected several variable sources in both UVOT and XRT data, but we related none of them to an SN SBO event.

This work demonstrates that the *Swift* satellite is suitable for carrying out targeted, multi-wavelength, time domain observations. We discussed the importance of the detection of X-ray/UV SBOs, which are difficult to detect, but can be a powerful tool with which to gain information about the progenitor star and the properties of the ejecta. Moreover, the onset of the SBO is the best EM mark of the moment of the explosion of massive stars. While the accuracy on the onset time provided by the study of canonical optical SNe and GRB afterglows cannot be better than about one day, for the X-ray/UV SBO it can be as accurate as a few hours down to seconds.

We stress that a survey like the one we carried out with *Swift* is and will be useful in the framework of multi-messenger astronomy. It can significantly contribute to the detection of EM signature of the GW sources. Indeed, SNe are putative GW emitters, and the detection of their SBO would increase our ability to constrain the time window in which the explosion takes place, which is crucial to search for GW signals. In addition, SNe occurring in dense circumstellar environment can be particularly bright in the X-rays (Chandra et al. 2012) with an emission that can be observable for weeks to months, providing a useful probe for the circumstellar matter properties and for the final stages of the progenitor star (Ofek et al. 2013).

Finally, all galaxies included in our sample are close enough (<50 Mpc) to lie within the a-LIGO and a-Virgo horizon for NS-NS and black hole-NS merger events. Despite the limited field of view of *Swift*/XRT and UVOT, choosing nearby galaxies as targets of a regular, periodic observation is a winning strategy to trigger the GW signal search, to find possible EM counterparts during follow-up of GW detections (see e.g. Evans et al. 2016), and to rule out contaminants by studying their light curves.

Acknowledgements. G.T., S.C., P.D.A., and A.M. acknowledge the support from ASI I/004/11/0. MB acknowledges financial support from the Italian Ministry of Education, University and Research (MIUR) through grant FIRB 2012 RBFR12PM1F. M.G.B. acknowledges the T-Rex project.

[14] `vizier.u-strasbg.fr/viz-bin/VizieR`

References

Abadie, J., Abbott, B. P., Abbott, R., et al. 2012a, ApJ, 760, 12
Abadie, J., Abbott, B. P., Abbott, R., et al. 2012b, A&A, 539, A124
Aasi, J., et al. (LIGO Scientific Collaboration and Virgo Collaboration) 2013, ArXiv e-prints [arXiv:1304.0670]
Aasi, J., Abbott, B. P., et al. 2015, Class. Quant. Grav., 32, 074001
Acernese, F., Agathos, M., Agatsuma, K., et al. 2015, Class. Quant. Grav., 32, 024001
Alard, C. 2000, A&AS, 144, 363
Alard, C., & Lupton, R. H. 1998, ApJ, 503, 325
Barbon, R., Buondí, V., Cappellaro, E., & Turatto, M. 1999, A&A, 139, 531
Bertin, E., & Arnouts, S. 2010, SExtractor: Source Extractor, Astrophysics Source Code Library [record ascl:1010.064]
Botticella, M. T., Cappellaro, E., Pignata, G., et al. 2013, The Messenger, 151, 29
Breeveld, A. A., Landsman, W., Holland, S. T., et al. 2011, in AIP Conf. Ser. 1358, eds. J. E. McEnery, J. L. Racusin, & N. Gehrels, 373
Brinkmann, W., Siebert, J., & Boller, T. 1994, A&A, 281, 355
Brough, S., Forbes, D. A., Kilborn, V. A., Couch, W., & Colless, M. 2006, MNRAS, 369, 1351
Campana, S., Mangano, V., Blustin, A. J., et al. 2006, Nature, 442, 1008
Cappellaro, E., Evans, R., & Turatto, M. 1999, A&A, 351, 459
Cavuoti, S., Brescia, M., D'Abrusco, R., Longo, G., & Paolillo, M. 2014, MNRAS, 437, 968
Chandra, P., Chevalier, R. A., Irwin, C. M., et al. 2012, ApJ, 750, L2
Chevalier, R. A., & Klein, R. I. 1978, ApJ, 219, 994
Colgate, S. A. 1974, ApJ, 187, 333
Cowperthwaite, P. S., & Berger, E. 2015, ApJ, 814, 25
Devillard, N. 1997, The Messenger, 87, 19
Drake, A. J., Djorgovski, S. G., Mahabal, A., et al. 2009, ApJ, 696, 870
Evans, P. A., Beardmore, A. P., Page, K. L., et al. 2009, MNRAS, 397, 1177
Evans, P. A., Fridriksson, J. K., Gehrels, N., et al. 2012, ApJS, 203, 28
Evans, P. A., Osborne, J. P., Kennea, J. A., et al. 2016, MNRAS, 455, 1522
Falk, S. W. 1978, ApJ, 225, L133
Flesch, E. 2010, PASA, 27, 283
Foley, R. J., Van Dyk, S. D., Jha, S. W., et al. 2015, ApJ, 798, L37
Fryer, C. L., & New, K. C. B. 2011, Living Rev. Relativity, 14, 1
Gehrels, N., & Cannizzo, J. K. 2015, J. High Energy Astrophysics, 7, 2
Gezari, S., Dessart, L., Basa, S., et al. 2008, ApJ, 683, L131
Gezari, S., Rest, A., Huber, M. E., et al. 2010, ApJ, 720, L77
Ghirlanda, G., Salvaterra, R., Campana, S., et al. 2015, A&A, 578, A71
Gossan, S. E., Sutton, P., Stuver, A., et al. 2015, ArXiv e-prints [arXiv:1511.02836]
Kanner, J., Camp, J., Racusin, J., Gehrels, N., & White, D. 2012, ApJ, 759, 22
Kanner, J., Baker, J., Blackburn, L., et al. 2013, ApJ, 774, 63
Kasliwal, M., Cao, Y., Surace, J., et al. 2013, SPIRITS: SPitzer InfraRed Intensive Transients Survey, Spitzer Proposal
Keller, S. C., Schmidt, B. P., Bessell, M. S., et al. 2007, PASA, 24, 1
Lonsdale, C. J., Diamond, P. J., Thrall, H., Smith, H. E., & Lonsdale, C. J. 2006, ApJ, 647, 185
Mannucci, F., Maiolino, R., Cresci, G., et al. 2003, A&A, 401, 519
Matzner, C. D., & McKee, C. F. 1999, ApJ, 510, 379
Müller, B., Janka, H.-T., & Marek, A. 2013, ApJ, 766, 43
Nakano, S., Itagaki, K., Guido, E., et al. 2014, CBET, 4011, 1
Ochner, P., Tomasella, L., Benetti, S., et al. 2014, ATel, 6648, 1
Ofek, E. O., Fox, D., Cenko, S. B., et al. 2013, ApJ, 763, 42
Ott, C. D. 2009, Classical and Quantum Gravity, 26, 063001
Ott, C. D., Abdikamalov, E., Mösta, P., et al. 2013, ApJ, 768, 115
Piro, A. L., & Nakar, E. 2014, ApJ, 784, 85
Poole, T. S., Breeveld, A. A., Page, M. J., et al. 2008, MNRAS, 383, 627
Ptak, A., Yaqoob, T., Serlemitsos, P. J., Kunieda, H., & Terashima, Y. 1996, ApJ, 459, 542
Ptak, A., Hornschemeier, A., Zezas, A., et al. 2015, ApJ, 800, 104
Rabinak, I., & Waxman, E. 2011, ApJ, 728, 63
Rabinowitz, D. L., Tourtellotte, S., Baltay, C., et al. 2011, in BAAS, 43, Am. Astron. Soc. Meet. Abstr., 217, 126.04
Rau, A., Kulkarni, S. R., Law, N. M., et al. 2009, PASP, 121, 1334
Roming, P. W. A., Kennedy, T. E., Mason, K. O., et al. 2005, Space Sci. Rev., 120, 95
Schawinski, K., Justham, S., Wolf, C., et al. 2008, Science, 321, 223
Shears, J., Boyd, D., Buczynski, D., et al. 2011, J. British Astron. Assoc., 121, 36
Singer, L. P., Price, L. R., Farr, B., et al. 2014, ApJ, 795, 105
Smartt, S. J. 2009, ARA&A, 47, 63
Soderberg, A. M., Berger, E., Page, K. L., et al. 2008, Nature, 453, 469
Spinelli, P. F., Storchi-Bergmann, T., Brandt, C. H., & Calzetti, D. 2006, ApJS, 166, 498
Stubbs, C. W., Doherty, P., Cramer, C., et al. 2010, ApJS, 191, 376
van den Bergh, S., Li, W., & Filippenko, A. V. 2005, PASP, 117, 773
Waagen, E. O. 2011, AAVSO Alert Notice, 446, 1
Waxman, E., Mészáros, P., & Campana, S. 2007, ApJ, 667, 351
Wąs, M., Sutton, P. J., Jones, G., & Leonor, I. 2012, Phys. Rev. D., 86, 022003
Willingale, R., Starling, R. L. C., Beardmore, A. P., Tanvir, N. R., & O'Brien, P. T. 2013, MNRAS, 431, 394
Zezas, A., Ward, M. J., & Murray, S. S. 2003, ApJ, 594, L31

Appendix A: Additional figures and tables

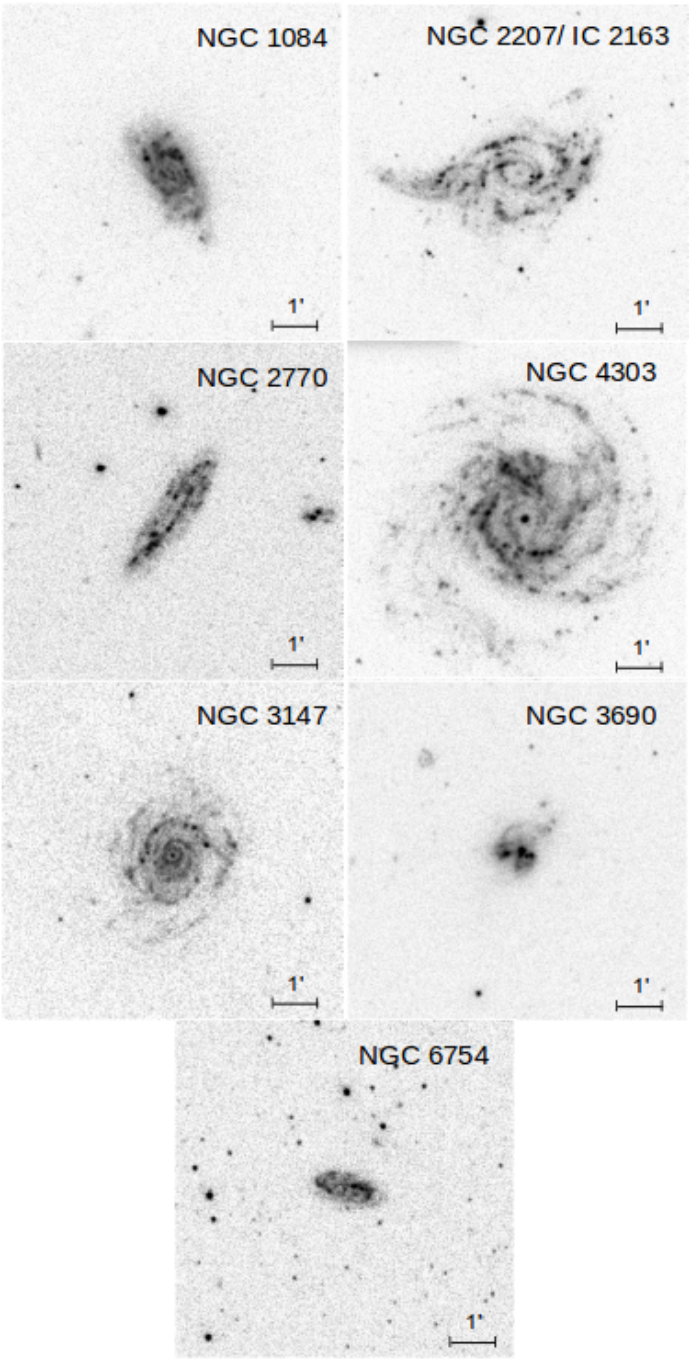

Fig. A.1. Single-epoch images taken with the *Swift*/UVOT of the target galaxies: NGC 1084, the system NGC 2207/IC 2163, NGC 2770, NGC 4303/M 61, NGC 3147, NGC 3690, and NGC 6754. The angular size of each image is $7' \times 7'$.

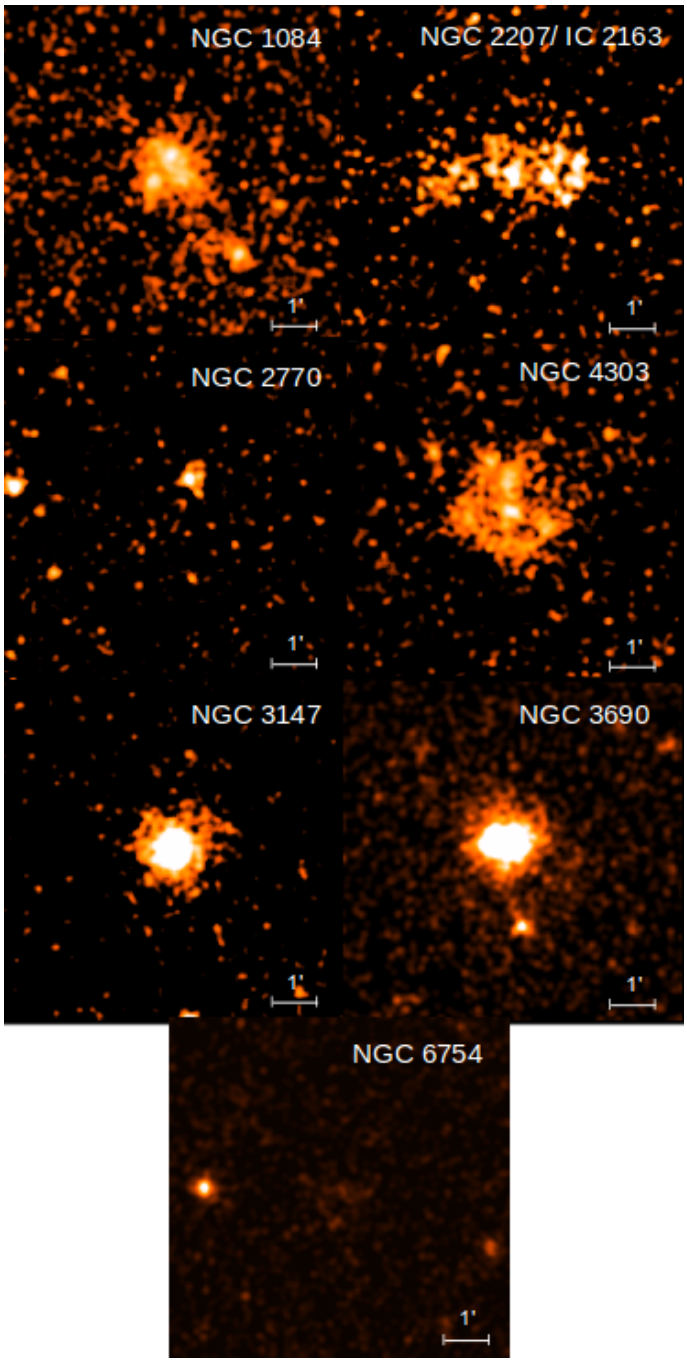

Fig. A.2. Sum of all the images taken with the *Swift*/XRT of the target galaxies: NGC 1084, the system NGC 2207/IC 2163, NGC 2770, NGC 4303/M 61, NGC 3147, NGC 3690, and NGC 6754. The angular size of each image is $7' \times 7'$.

Table A.1. Identification number, starting date, and exposure time of observations carried out by the *Swift* instruments XRT and UVOT during the monitoring of NGC 1084.

NGC 1084

Obs ID	Obs date	X-ray exposure	UV exposure
32999001	2013-11-01	1.5E+03 s	–
32999002	2013-11-09	1.9E+03 s	1.8E+03 s
32999003	2013-11-17	2.0E+03 s	2.0E+03 s
32999004	2013-11-23	1.9E+03 s	1.9E+03 s
32999005	2013-11-30	2.2E+03 s	2.2E+03 s
32999006	2013-12-07	2.0E+03 s	2.0E+03 s
32999007	2013-12-14	1.9E+03 s	1.9E+03 s
32999008	2013-12-21	1.9E+03 s	1.9E+03 s
32999009	2013-12-28	1.9E+03 s	1.9E+03 s
32999010	2014-01-04	2.2E+03 s	2.2E+03 s
32999011	2014-01-11	1.8E+03 s	1.8E+03 s
32999012	2014-01-18	2.0E+03 s	2.0E+03 s
32999013	2014-01-25	1.9E+03 s	1.9E+03 s
32999014	2014-02-01	2.1E+03 s	2.1E+03 s
32999015	2014-02-08	1.9E+03 s	1.9E+03 s
32999016	2014-02-15	1.9E+03 s	1.8E+03 s
32999017	2014-02-22	1.8E+03 s	1.8E+03 s
32999018	2014-03-01	1.9E+03 s	1.8E+03 s
32999019	2014-03-08	2.2E+03 s	2.2E+03 s
32999020	2014-03-13	2.0E+03 s	1.1E+03 s

Table A.2. Identification number, starting date, and exposure time of observations carried out by the *Swift* instruments XRT and UVOT during the monitoring of the system NGC 2207/IC 2163.

NGC 2207/IC 2163

Obs ID	Obs date	X-ray exposure	UV exposure
33002001	2013-11-03	1.6E+03 s	1.6E+03 s
33002002	2013-11-10	2.0E+03 s	–
33002003	2013-11-17	1.9E+03 s	1.9E+03 s
33002004	2013-11-24	1.9E+03 s	1.9E+03 s
33002005	2013-12-01	2.2E+03 s	2.2E+03 s
33002007	2013-12-11	1.8E+03 s	1.8E+03 s
33002008	2013-12-15	2.2E+03 s	2.2E+03 s
33002009	2013-12-22	1.7E+03 s	1.8E+03 s
33002010	2013-12-29	1.4E+03 s	1.3E+03 s
33002011	2014-01-05	1.9E+03 s	1.9E+03 s
33002012	2014-01-12	2.0E+03 s	1.9E+03 s
33002013	2014-01-19	1.9E+03 s	1.9E+03 s
33002014	2014-01-26	2.0E+03 s	2.0E+03 s
33002015	2014-02-02	2.1E+03 s	2.1E+03 s
33002016	2014-02-09	1.9E+03 s	1.9E+03 s
33002017	2014-02-16	2.1E+03 s	2.1E+03 s
33002018	2014-02-23	1.3E+03 s	1.3E+03 s
33002019	2014-02-26	1.2E+03 s	1.2E+03 s
33002020	2014-03-02	2.0E+03 s	2.0E+03 s
33002021	2014-03-09	2.2E+03 s	2.2E+03 s
33002022	2014-03-16	1.8E+03 s	1.8E+03 s
33002023	2014-03-23	1.8E+03 s	1.8E+03 s
33002024	2014-03-30	2.0E+03 s	2.0E+03 s
33002025	2014-04-06	2.0E+03 s	2.0E+03 s
33002026	2014-04-13	1.9E+03 s	1.9E+03 s
33002027	2014-04-20	2.2E+03 s	2.2E+03 s
33002028	2014-04-27	2.0E+03 s	2.0E+03 s

Table A.3. Identification number, starting date, and exposure time of observations carried out by the *Swift* instruments XRT and UVOT during the monitoring of NGC 2770.

NGC 2770

Obs ID	Obs date	X-ray exposure	UV exposure
33000001	2013-12-10	2.0E+03 s	2.0E+03 s
33000002	2013-12-17	2.0E+03 s	1.9E+03 s
33000003	2013-12-24	2.0E+03 s	1.9E+03 s
33000004	2013-12-31	2.0E+03 s	1.9E+03 s
33000005	2014-01-07	1.9E+03 s	1.9E+03 s
33000007	2014-01-16	1.9E+03 s	1.9E+03 s
33000008	2014-01-21	2.2E+03 s	2.2E+03 s
33000009	2014-01-28	1.8E+03 s	1.8E+03 s
33000010	2014-02-04	1.5E+03 s	1.5E+03 s
33000011	2014-02-11	2.0E+03 s	-
33000012	2014-02-18	2.0E+03 s	1.9E+03 s
33000013	2014-02-25	2.7E+03 s	2.7E+03 s
33000014	2014-03-04	1.8E+03 s	1.8E+03 s
33000015	2014-03-11	2.2E+03 s	2.2E+03 s
33000016	2014-03-18	1.7E+03 s	1.7E+03 s
33000017	2014-03-25	2.6E+03 s	2.6E+03 s
33000018	2014-04-01	2.2E+03 s	2.2E+03 s
33000019	2014-04-07	1.9E+03 s	2.1E+03 s
33000020	2014-04-15	1.8E+03 s	1.8E+03 s
33000021	2014-04-22	2.2E+03 s	2.2E+03 s
33000023	2014-05-02	2.2E+03 s	2.2E+03 s
33000024	2014-05-07	1.9E+03 s	1.9E+03 s
33000025	2014-05-13	1.9E+03 s	1.8E+03 s
33000026	2014-05-20	2.2E+03 s	2.2E+03 s
33000027	2014-05-27	1.9E+03 s	1.8E+03 s
33000028	2014-06-04	–	2.1E+03 s

Table A.4. Identification number, starting date, and exposure time of observations carried out by the *Swift* instruments XRT and UVOT during the monitoring of NGC 4303.

NGC 4303

Obs ID	Obs date	X-ray exposure	UV exposure
33001001	2014-01-24	2.0E+03 s	2.0E+03 s
33001003	2014-02-06	1.6E+03 s	1.6E+03 s
33001004	2014-02-13	2.1E+03 s	2.0E+03 s
33001005	2014-02-20	2.0E+03 s	1.9E+03 s
33001006	2014-02-27	8.2E+02 s	8.3E+02 s
33001007	2014-03-04	1.9E+03 s	1.9E+03 s
33001008	2014-03-06	2.2E+03 s	–
33001009	2014-03-13	1.7E+03 s	–
33001010	2014-03-20	2.0E+03 s	1.9E+03 s
33001011	2014-03-27	2.0E+03 s	2.0E+03 s
33001012	2014-03-27	2.9E+03 s	8.8E+02 s
33001013	2014-03-28	4.7E+03 s	1.1E+03 s
33001014	2014-04-03	2.0E+03 s	1.9E+03 s
33001015	2014-04-10	1.5E+03 s	1.4E+03 s
33001016	2014-04-17	2.1E+03 s	1.6E+03 s
33001017	2014-04-24	1.9E+03 s	1.9E+03 s
33001018	2014-05-01	1.7E+03 s	1.7E+03 s
33001019	2014-05-08	2.2E+03 s	2.1E+03 s
33001020	2014-05-15	1.3E+03 s	1.3E+03 s
33001021	2014-05-22	2.0E+03 s	2.0E+03 s
33001022	2014-05-29	2.1E+03 s	1.0E+03 s
33001023	2014-06-04	–	1.9E+03 s

Table A.5. Identification number, starting date, and exposure time of observations carried out by the *Swift* instruments XRT and UVOT during the monitoring of NGC 3690.

NGC 3690

Obs ID	Obs date	X-ray exposure	UV exposure
32998001	2014-01-10	1.9E+03 s	1.9E+03 s
32998002	2014-01-17	1.9E+03 s	–
32998003	2014-01-24	2.2E+03 s	2.2E+03 s
32998004	2014-01-31	1.9E+03 s	1.9E+03 s
32998005	2014-02-07	2.0E+03 s	2.0E+03 s
32998006	2014-02-14	1.4E+03 s	1.4E+03 s
32998007	2014-02-21	5.2E+03 s	–
32998008	2014-02-26	9.5E+02 s	9.5E+02 s
32998009	2014-02-28	1.7E+03 s	1.8E+03 s
32998010	2014-03-07	2.1E+03 s	2.1E+03 s
32998011	2014-03-14	1.8E+03 s	1.9E+03 s
32998012	2014-03-21	1.7E+03 s	1.6E+03 s
32998013	2014-03-28	1.9E+03 s	1.9E+03 s
32998014	2014-04-04	2.1E+03 s	2.1E+03 s
32998015	2014-04-11	2.2E+03 s	2.2E+03 s
32998016	2014-04-18	1.7E+03 s	1.6E+03 s
32998017	2014-04-25	1.5E+03 s	1.5E+03 s
32998018	2014-05-02	1.5E+03 s	1.5E+03 s
32998020	2014-05-16	1.9E+03 s	1.8E+03 s
32998021	2014-05-23	2.0E+03 s	2.0E+03 s
32998022	2014-05-30	2.3E+03 s	2.3E+03 s
32998023	2014-06-06	–	2.0E+03 s
32998024	2014-06-13	1.9E+03 s	1.9E+03 s
32998025	2014-06-20	1.9E+03 s	1.9E+03 s
32998026	2014-06-27	1.5E+03 s	1.5E+03 s
32998027	2014-07-04	1.8E+03 s	1.8E+03 s
32998028	2014-07-11	2.0E+03 s	2.0E+03 s
32998029	2014-07-18	2.2E+03 s	2.2E+03 s
32998030	2014-07-25	1.9E+03 s	1.9E+03 s
32998031	2014-08-08	2.1E+03 s	2.1E+03 s
32998032	2014-08-15	1.9E+03 s	1.9E+03 s
32998033	2014-08-22	2.7E+03 s	2.0E+03 s
32998034	2014-08-29	2.1E+03 s	2.1E+03 s
32998035	2014-09-05	1.8E+03 s	1.8E+03 s
32998037	2014-09-18	2.1E+03 s	2.1E+03 s
32998038	2014-09-26	1.9E+03 s	1.9E+03 s

Table A.6. Identification number, starting date, and exposure time of observations carried out by the *Swift* instruments XRT and UVOT during the monitoring of NGC 6754.

NGC 6754

Obs ID	Obs date	X-ray exposure	UV exposure
33225001	2014-04-06	1.8E+03 s	1.7E+03
33225002	2014-04-13	2.0E+03 s	2.0E+03
33225003	2014-04-20	2.1E+03 s	2.1E+03
33225004	2014-04-27	1.7E+03 s	1.6E+03
33225005	2014-05-04	2.1E+03 s	2.1E+03
33225006	2014-05-11	2.0E+03 s	2.0E+03
33225007	2014-05-18	1.7E+03 s	1.7E+03
33225008	2014-05-25	2.0E+03 s	2.0E+03
33225009	2014-06-01	2.0E+03 s	2.0E+03
33225011	2014-06-15	2.0E+03 s	2.0E+03
33225012	2014-06-22	1.7E+03 s	1.7E+03
33225013	2014-06-29	2.0E+03 s	1.9E+03
33225014	2014-07-06	2.1E+03 s	2.0E+03
33225015	2014-07-13	1.7E+03 s	1.7E+03
33225016	2014-07-17	1.7E+03 s	1.7E+03
33225017	2014-07-20	2.3E+03 s	2.2E+03
33225018	2014-07-27	1.9E+03 s	1.9E+03
33225019	2014-08-03	1.9E+03 s	1.9E+03
33225020	2014-08-10	2.2E+03 s	2.2E+03
33225021	2014-08-17	2.4E+03 s	2.4E+03
33225022	2014-08-24	5.9E+02 s	5.9E+02
33225023	2014-08-31	6.1E+02 s	6.2E+02
33225024	2014-09-04	1.4E+03 s	1.4E+03
33225025	2014-09-07	2.0E+03 s	2.0E+03
33225026	2014-09-14	1.9E+03 s	1.9E+03
33225027	2014-09-21	3.1E+03 s	3.1E+03
33225028	2014-09-28	2.0E+03 s	2.0E+03

Table A.7. Identification number, starting date, and exposure time of observations carried out by the *Swift* instruments XRT and UVOT during the monitoring of NGC 3147.

NGC 3147				
Obs ID	Obs date	X-ray exposure	UV exposure	Index (0.3−10 KeV)
37992002	2013-12-25	1.8E+03 s	1.8E+03 s	1.7 (+0.4, −0.4)
37992003	2014-01-01	1.9E+03 s	1.9E+03 s	1.31 (+0.45, −0.17)
37992004	2014-01-15	2.1E+03 s	2.1E+03 s	1.25 (+0.34, −0.21)
37992005	2014-01-22	2.1E+03 s	2.1E+03 s	1.17 (+0.34, −0.17)
37992006	2014-01-29	1.9E+03 s	1.9E+03 s	1.30 (+0.39, −0.29)
37992007	2014-02-05	2.0E+03 s	2.0E+03 s	1.7 (+0.5, −0.4)
37992008	2014-02-12	1.8E+03 s	1.7E+03 s	1.6 (+0.4, −0.4)
37992009	2014-02-19	2.1E+03 s	2.1E+03 s	1.49 (+0.31, −0.22)
37992010	2014-03-06	1.9E+03 s	2.1E+03 s	1.48 (+0.36, −0.29)
37992011	2014-03-12	6.1E+02 s	6.2E+02 s	1.5 (+0.8, −0.6)
37992012	2014-03-16	1.4E+03 s	1.4E+03 s	1.4 (+0.5, −0.3)
37992013	2014-03-19	2.0E+03 s	2.0E+03 s	1.48 (+0.43, −0.28)
37992014	2014-03-26	2.2E+03 s	2.2E+03 s	1.47 (+0.39, −0.29)
37992015	2014-04-02	1.8E+03 s	1.8E+03 s	1.66 (+0.48, −0.29)
37992016	2014-04-09	2.3E+03 s	2.3E+03 s	1.52 (+0.39, −0.15)
37992017	2014-04-16	1.8E+03 s	1.7E+03 s	1.38 (+0.34, −0.17)
37992018	2014-04-26	1.3E+03 s	1.3E+03 s	1.7 (+0.5, −0.4)
37992019	2014-04-30	1.7E+03 s	1.7E+03 s	2.0 (+0.6, −0.5)
37992020	2014-05-07	1.9E+03 s	1.9E+03 s	1.8 (+0.4, −0.4)
37992021	2014-05-14	2.0E+03 s	1.9E+03 s	1.42 (+0.28, −0.23)
37992022	2014-05-21	2.2E+03 s	2.2E+03 s	1.33 (+0.43, −0.22)
37992023	2014-05-28	2.1E+03 s	2.1E+03 s	1.49 (+0.45, −0.26)
37992024	2014-06-04	–	2.2E+03 s	–
37992026	2014-06-22	2.1E+03 s	2.1E+03 s	1.9 (+0.5, −0.5)
37992027	2014-06-25	1.9E+03 s	1.9E+03 s	1.42 (+0.51, −0.22)
37992028	2014-07-02	2.1E+03 s	2.1E+03 s	1.6 (+0.5, −0.3)
37992029	2014-07-09	1.3E+03 s	–	1.5 (+0.5, −0.4)
37992030	2014-07-13	1.0E+03 s	1.0E+03 s	1.9 (+0.6, −0.5)

Notes. In the last column, the photon index of the absorbed power-law spectrum computed (through the *Swift*/XRT online tools; Evans et al. 2009) in the XRT 0.3−10 KeV with a Galactic column density of 3.30×10^{20} cm^{-2} (Willingale et al. 2013).